RSC Advances

PAPER

View Article Online
View Journal | View Issue

Cite this: *RSC Adv.*, 2016, **6**, 68739

Mesoporous SnO_2–SiO_2 and Sn–silica–carbon nanocomposites by novel non-hydrolytic templated sol–gel synthesis†

David Skoda,[ab] Ales Styskalik,[ab] Zdenek Moravec,[a] Petr Bezdicka,[c] Jiri Bursik,[d] P. Hubert Mutin[e] and Jiri Pinkas*[ab]

A novel non-hydrolytic sol–gel (NHSG) synthesis of mesoporous tin silicate xerogels is presented. The polycondensation between silicon tetraacetate, $Si(OAc)_4$, and tetrakis(diethylamido)tin, $Sn(NEt_2)_4$, resulting in acetamide elimination leads to tin silicate xerogels containing Si–O–Sn linkages. The addition of Pluronic P123 or F127 templates provides homogeneous stiff gels that are, after template removal by calcination at 500 °C in air, converted to stable mesoporous silica xerogels with large surface areas (476 $m^2\ g^{-1}$) and dispersed SnO_2 nanoparticles (6–7 nm). Heat treatment of the as-prepared tin silicate gels in an inert N_2 atmosphere leads to reduction and transformation to Sn nanoparticles (70–150 nm) embedded in a silica–carbon matrix. The composition and morphology of the xerogels, volatile reaction byproducts, and thermal transformations were followed by elemental analyses, IR spectroscopy, thermal analysis TG-DSC, nitrogen adsorption measurements, solid-state NMR spectroscopy, DRUV-vis spectroscopy, electron microscopy, and HT powder XRD. The SnO_2–SiO_2 xerogels were tested as potential catalysts for aminolysis of styrene oxide with aniline and for the Meerwein–Ponndorf–Verley reduction of 4-*tert*-butylcyclohexanone. The resulting reaction systems displayed good activity and selectivity.

Received 27th June 2016
Accepted 12th July 2016

DOI: 10.1039/c6ra16556g

www.rsc.org/advances

Introduction

Silicates containing tin have attracted much attention due to their surface acidity and catalytic activity in a variety of reactions (hydroxylation of phenols,[1] Baeyer–Villiger oxidations,[2] Meerwein–Ponndorf–Verley reductions,[3] sugar isomerization,[4] epimerization,[5] oxidative dehydrogenation of cyclohexane,[6] and Cannizzaro-type reactions[7]). SnO_2/SBA-15 materials or SnO_2–SiO_2 nanocomposites were studied as gas sensors,[8] photocatalysts for rhodamine B degradation[9,10] or catalysts for benzylation of aromatics[11] and C–C coupling reactions.[12] The efficiency of these processes increases with the specific surface area of SnO_2 particles. The factors which influence the surface area, such as primary particle diameter and state of aggregation of the particles, are of great interest.[13] In order to prepare individual primary particles with diameters below 10 nm, and avoid their aggregation, templates based on porous materials are widely used as supports in nanoparticle synthesis.[9,14]

Many reports are devoted to porous materials such as Sn-ZSM12, Sn-beta zeolites, Sn-MFI, Sn-MCM, Sn-SBA, and Sn-KIT-5.[2,4,8,12,15–17] Preparation procedures for mesoporous tin silicate materials involve addition of a tin precursor ($SnCl_2$, $SnCl_4 \cdot 5H_2O$) into an appropriate mesoporous silica (MCM, SBA, KIT-5) reaction mixture. Aqueous solutions of TEOS with HCl and Pluronic P123 or F127 are used in the case of SBA or KIT-5 supports.[8,18] The resulting mesoporous tin silicates were used in a variety of catalytic reactions and they displayed high activities. For example, Endud used Sn-MCM-48 molecular sieve (1291–1585 $m^2\ g^{-1}$) as a catalyst for oxidation of benzyl alcohol with TBHP.[17] An interesting method for the preparation of nanocrystalline Sn-beta zeolite catalysts for ring-opening hydration of epoxides was published by Tang.[16] This approach is based on dealumination of commercial beta aluminosilicate zeolite with nitric acid and a subsequent reaction with $(CH_3)_2SnCl_2$. Recently, Reddy successfully applied mesoporous (582–732 $m^2\ g^{-1}$) tin silicates as catalysts for acyl Sonogashira coupling reactions with yields up to 97%.[12]

The major problem of hydrolytic sol–gel processes is the disparity in the hydrolysis reaction rates of different precursors. The non-hydrolytic method[19–21] involves completely different mechanism of polycondensation reactions in non-aqueous media and offers decisive advantages, such as control of

[a]*Masaryk University, Department of Chemistry, Kotlarska 2, CZ-61137 Brno, Czech Republic. E-mail: jpinkas@chemi.muni.cz*
[b]*Masaryk University, CEITEC MU, Kamenice 5, CZ-62500 Brno, Czech Republic*
[c]*Institute of Inorganic Chemistry ASCR, CZ-25068 Husinec-Rez, Czech Republic*
[d]*Institute of Physics of Materials ASCR, Zizkova 22, CZ-616 62 Brno, Czech Republic*
[e]*Institut Charles Gerhardt UMR 5253 CNRS-UM-ENSCM, Université de Montpellier, Place Eugène Bataillon, 34095 Montpellier Cedex 05, France*

† Electronic supplementary information (ESI) available. See DOI: 10.1039/c6ra16556g

composition, homogeneity, structure, and texture.[22] However, the non-aqueous synthesis of SnO_2–SiO_2 materials is not well developed and only two reports were published on this topic. The first describes a procedure based on the reaction of TEOS with tin(IV) acetate in anhydrous acetic acid.[23] The second report introduces the twin polymerization method for the production of SnO_2–SiO_2 materials.[24] When compared to conventional hydrolytic methods, non-hydrolytic sol–gel chemistry provides effective routes for the synthesis of homogeneous monolithic gels, nanoparticles[25] and heterogeneous catalysts.[19,20]

We have recently reported that non-hydrolytic acetamide elimination[26] can be successfully used for the synthesis of mesoporous titanosilicate, zirconium silicate, and aluminosilicate catalysts.[27–29] In the work presented here, this reaction was used for the preparation of tin silicate xerogels. Templated one-pot sol–gel method provided homogeneous stiff gels with a high content of Sn. We were also able to prepare SnO_2 nanoparticles embedded in mesoporous silica matrix which prevented them from aggregation. Resulting SnO_2–SiO_2 xerogels were tested as catalysts for aminolysis of styrene oxide. Heating of dried gels in nitrogen at 500 °C caused reduction of Sn(IV) species and Sn–silica–carbon nanocomposites were obtained.

Experimental

General procedures

All manipulations were performed in an atmosphere of dry nitrogen using Schlenk techniques or in an M. Braun dry box with both H_2O and O_2 levels below 1 ppm.

Chemicals, such as Pluronic P123 ($EO_{20}PO_{70}EO_{20}$, M_{av} = 5845 g mol^{-1}), Pluronic F127 ($EO_{100}PO_{65}EO_{100}$, M_{av} = 12 600 g mol^{-1}), tetrakis(diethylamido)tin $Sn(NEt_2)_4$ (99%), styrene oxide (97%), aniline (97%), 4-*tert*-butylcyclohexanone (99%), and nonane (99%), were purchased from Sigma-Aldrich. $Si(OAc)_4$ was synthesized according to the published procedure.[30] Toluene, dichloromethane and isopropanol were dried by standard methods and distilled before use. Pluronic P123 and F127 were dried under vacuum at 60 °C and dissolved in dry toluene and stored as 20 wt% solutions.

Synthesis of tin silicates

Tin silicate xerogels were synthesized by templated acetamide elimination according to eqn (1).

SiSnF – at ambient pressure

$Sn(NEt_2)_4$ (1.229 g; 3.054 mmol) was added dropwise with a syringe to a stirred solution of $Si(OAc)_4$ (0.789 g; 2.99 mmol) and Pluronic F127 (1.92 g; 0.152 mmol) in toluene (40 cm^3). After the addition, the color changed to light orange-yellow. The reaction mixture was heated to 80 °C and a transparent light yellow-brown stiff gel was formed after 20 min. The reaction temperature was maintained for 168 h, then the volatile byproducts were separated *in vacuo* and the solid product (yellow gel) was dried under vacuum for 24 h. Yield 3.074 g, DC% = 59%.

Identification of volatile by-products. GC-MS: 3.6 min (*N*,*N*-diethylacetamide), m/z = 115, 100, 72, 58, 44.

Characterization of dried xerogel. IR (ATR, cm^{-1}): 555 w, 669 w (ν Sn–O–Sn), 799 w, 845 w, 953 s (ν Si–O–Sn), 1027 s (ν Si–O–Si), 1099 vs (δ C–O–C), 1252 w (ν C–N–C), 1300 w, 1353 w, 1372 m (δ CH_3), 1453 m (ν_{sym} COO), 1564 m (ν_{asym} COO), 1639 w (ν C═O, acetamide), 2870 m (ν CH), 2971 w (ν CH).

TG/DSC: (air, 5 °C min^{-1}) weight loss at 1000 °C 69.40%; (N_2, 5 °C min^{-1}) weight loss at 1000 °C 69.21%.

SiSnF dried xerogel was calcined in a tube furnace at 400 (SiSnF-400) and 500 °C (SiSnF-500) for 3 h in air to remove the template. Carbonization of template and reduction of Sn species was performed by heat treatment under N_2 at 400 (SiSnF-400N) or 500 °C (SiSnF-500N) for 3 h.

Characterization of calcined xerogel. ICP-OES (wt%): SiSnF-500 (500 °C, air) Sn 43.2 ± 0.5, Si 11.6 ± 0.1; SiSnF-500N (500 °C, N_2) Sn 61.5 ± 0.6, Si 11.6 ± 0.2, elemental analyses (wt%): SiSnF-500N (500 °C, N_2) C 13.17, H 0.60.

MAS NMR SiSnF-500 (500 °C, air): ^{29}Si CPMAS (ppm), δ −110, −102, −92.

BET SiSnF-500 (500 °C, air) 191 m^2 g^{-1}, C = 94, V_{tot} = 0.39 cm^3 g^{-1}, d = 9.8 nm.

SiSnP – at ambient pressure

The synthesis with Pluronic P123 was carried out in analogous manner. Results of analytical measurements are discussed in later sections.

SiSnPA – in an autoclave (autogenous pressure)

$Si(OAc)_4$ (0.405 g, 1.53 mmol) was dissolved in CH_2Cl_2 (18 cm^3) and mixed with P123 (0.39 g, 0.067 mmol) solution in toluene (2.0 g of solution, 19.7 wt%). Then $Sn(NEt_2)_4$ (0.459 g, 1.12 mmol) was added and the reaction mixture was sealed in a Teflon-lined autoclave. The autoclave was heated in an oven at 110 °C. After 5 days the reaction was stopped and the autoclave was opened in a glove box. The liquid phase was separated and the resulting gel was placed into a Schlenk flask and dried under vacuum. Yield: 0.591 g.

Identification of volatile by-products. GC-MS: 3.5 min (*N*,*N*-diethylacetamide), m/z = 115, 100, 72, 58, 44.

Characterization of dried xerogel. IR (ATR, cm^{-1}): 493 w, 604 vw, 669 w (ν Sn–O–Sn), 796 w, 864 w, 943 s (ν Si–O–Sn), 1014 s (ν Si–O–Si), 1034 s (ν Si–O–Si), 1089 vs (δ C–O–C), 1252 w (ν C–N–C), 1300 w, 1372 m (δ CH_3), 1451 m (ν_{sym} COO), 1565 w (ν_{asym} COO), 1639 w (ν C═O, acetamide), 2869 m (ν CH), 2931 w (ν CH), 2971 w (ν CH).

TG/DSC: (air, 5 °C min^{-1}) weight loss at 1000 °C 61.71%; (N_2, 5 °C min^{-1}) weight loss at 1000 °C 61.45%.

Characterization of calcined xerogel SiSnPA-500 (500 °C, air). ICP-OES (wt%): Sn 35.5 ± 0.2, Si 19.0 ± 0.1.

MAS NMR: ^{29}Si CPMAS (ppm), δ −109, −102.

BET: 476 m^2 g^{-1}, C = 80, V_{tot} = 0.58 cm^3 g^{-1}, d = 6.6 nm.

Catalytic reactions

Calcined tin silicate xerogels were degassed before the reaction under vacuum at 115 °C for 20 min.

The MPV reduction[31] of 4-*tert*-butylcyclohexanone was carried out in a 50 cm^3 round-bottom Schlenk flask equipped with a reflux condenser connected to a dry N_2 source. The reaction mixture containing the calcined tin silicate catalyst (25 mg), 4-*tert*-butylcyclohexanone (500 mg, 3.54 mmol), and dry 2-propanol (15 cm^3, 0.20 mol) was stirred under reflux for 1 h.

Aminolysis of styrene oxide[32] was performed in a 25 cm^3 round-bottom Schlenk flask connected to a dry N_2 source. The reaction mixture consisted of a calcined tin silicate xerogel (25 mg), dry toluene (5 cm^3), aniline (0.456 cm^3, 5.00 mmol), and styrene oxide (0.587 cm^3, 5.00 mmol). This reaction mixture was heated at 50 °C for 1 h.

The products were analyzed by ^{1}H NMR spectroscopy and the GC-MS method using 0.100 cm^3 of nonane as an internal standard.

Characterization

IR spectra were recorded on a Bruker Tensor 27 FTIR spectrometer using KBr pellets or on a Bruker Alpha-Platinum ATR system. GC-MS measurements were performed on a mass spectrometer TSQ Quantum XLS coupled with a gas chromatograph Trace GC Ultra by Thermo Scientific. The gas chromatograph was equipped with a TS-SQC column (length 15 m, diameter 0.25 mm, film thickness 0.25 μm) using a temperature program: 50 °C (0 min), 5 °C min^{-1} to 80 °C, 15 °C min^{-1} ramp to 120 °C, 35 °C min^{-1} ramp to 200 °C, held at this temperature for 0.5 min. Injection split mode, injector, the interface, and detector temperatures were all set to 200 °C. The column pressure was 31.5 kPa and the ionization energy was 70 eV. For liquid phase ^{1}H and ^{13}C NMR measurements, a Bruker Avance III DRX 300 MHz spectrometer was used. The spectra were referenced to the residual proton or carbon resonances of benzene-d_6 (7.15 and 128.0 ppm) and $CDCl_3$ (7.20 and 77.0 ppm). ^{29}Si solid state NMR spectra were measured on a Bruker Avance III HD 700 MHz spectrometer with a MAS DVT 700S4 BL4 N-P/H probe. Chemical shifts were referenced externally to ^{29}Si δ [$(Me_3SiO)_8Si_8O_{20}$]: 11.72 ppm; ^{13}C δ [adamantane] 38.68 ppm. High temperature powder XRD diffractograms were recorded on an X'Pert PRO diffractometer equipped with a $Co_{K\alpha}$ X-ray tube and a HTK 16 high-temperature chamber (Anton Paar, Graz, Austria) with a Pt holder. Samples were measured from 500 to 1250 °C in 50 °C increments. The sample was held during scanning at a constant temperature for 12 min. Powder diffraction patterns were collected with the PANalytical X'Pert PRO diffractometer equipped with conventional X-ray tube (Cu K_α radiation, 40 kV, 30 mA) and a linear position sensitive detector PIXcel with an anti-scatter shield. Qualitative analysis was performed with HighScorePlus software package (PANalytical, The Netherlands, version 4.1.0), and Match3. For quantitative analysis of samples, we used Diffrac-Plus Topas (Bruker AXS, Germany, version 4.2). This program permits to estimate the weight fractions of crystalline phases by means of Rietveld refinement procedure.[33] Nitrogen adsorption/desorption experiments were performed at 77 K on a Quantachrome Autosorb-1MP porosimeter. Surface areas (SA) and total pore volumes (V_{tot} at $p/p_0 = 0.98$) were determined by volumetric techniques.[34,35] Prior to the measurements, the samples were degassed at 100 °C for at least 24 h until the outgas rate was less than 0.4 Pa min^{-1}. The adsorption–desorption isotherms were measured for each sample at least three times. The specific surface area was determined by the multipoint BET method using at least five data points with relative pressures between 0.05 and 0.30.[34,35] The valid pressure ranges were established by the Rouquerol transform and equivalent BET surface areas were calculated. Pore size distributions were calculated by the NLDFT method from the adsorption branch of the isotherms with the use of a nitrogen-on-silica kernel and by the QSDFT method for carbonized samples. Thermal analysis (TG/DSC) was performed on a Netzsch STA 449C Jupiter apparatus in a stream of air (70 cm^3 min^{-1}) with a temperature gradient of 5 °C min^{-1} to 1000 °C, in a Pt/Rh crucibles. Tin and silicon contents were determined on an ICP optical emission spectrometer iCAP 6500 Duo (Thermo, UK) equipped with a solid-state generator with a frequency of 27.12 MHz and a maximum power input 1350 W. For Si analysis, wavelengths of 212.4 and 251.6 nm were used. Sn was measured at 189.9 nm. Elemental analysis (C, H, and N) was performed on a Flash 2000 CHNS Elemental Analyzer (Thermo Scientific) at Palacky University, Olomouc. TEM images were obtained from a Philips CM 12 TEM/STEM system with EDAX Phoenix EDS, and JEOL JEM2010 and 3010 microscopes equipped with EDX detectors and CCD with resolution 1024 × 1024 pixels. Studies of surface acidity were performed on air-calcined xerogels (cca 50 mg) which were dried under vacuum (1 h, 115 °C) before adsorption. Then, the samples were exposed for 30 min to pyridine vapors under its autogenous pressure at 25 °C. After adsorption, samples were dried under vacuum at r.t. for 2 hours. Adsorbed pyridine was characterized by the IR technique.

In the template-assisted reactions between $Si(OAc)_4$ and $Sn(NEt_2)_4$, the yield of the product as well as the mass of starting precursors were precisely weighed to allow gravimetric estimation of the degree of condensation, $DC = 100(n_{total} - n_{residual})/n_{total}$, where n_{total} is the molar amount of organic groups in the starting materials and $n_{residual}$ is molar amount of residual organic groups in the xerogel is based on the difference of theoretical and experimental yield. As the condensation reactions were never quantitative, the degree of condensation represents the relative difference between the maximum theoretical loss of $Et_2NC(O)CH_3$ (eqn (1)) in comparison to what is experimentally observed. This difference also defines the number of acetoxy groups on silicon and diethylamide groups on tin that are left in the matrix.

Results and discussion

Tin silicate xerogels were synthesized by novel non-hydrolytic acetamide elimination according to eqn (1). We successfully applied this approach for the sol–gel synthesis of titanosilicates, zirconium silicates, and aluminosilicates. This polycondensation results in the formation of gels containing Si–O–M (M = Ti, Zr, Al) networks.[26–29] These xerogels are unfortunately microporous and after calcination nonporous. A significant

improvement is achieved with the addition of block-copolymer templates (Pluronic P123, F127) as structure directing agents. This modification allows obtaining stiff transparent gels. The templates are then removed by calcination in air at 500 °C and the final products exhibit mesoporous character with high surface areas. In this work we apply template-assisted acetamide elimination for the preparation of mesoporous tin silicates. The stoichiometric equation represents a complete polycondensation leading to the Si–O–Sn network and quantitative elimination of *N*,*N*-diethylacetamide. However, under experimental conditions, the condensation is incomplete and unreacted acetate and amide functional groups were observed in the xerogels. The reaction parameters are summarized in Table 1. For the comparison and modification of textural properties and surface areas, the reaction was performed also in a Teflon-lined autoclave in dry CH_2Cl_2 solvent. The precursors were mixed together in the autoclave inside a glove box. Then, the autoclave was placed into an oven and heated at 110 °C.

$$Si(OAc)_4 + Sn(NEt_2)_4 \rightarrow SiO_2–SnO_2 + 4Et_2NAc \quad (1)$$

The degrees of condensation (DC, %) for SiOSn xerogels (eqn (1)) determined by gravimetry reached 69% (Table 1).

All reactions proceed with the formation of transparent yellowish gels which are dried under vacuum to dark orange rubbery products. GC-MS analysis of volatile byproducts confirmed *N*,*N*-diethylacetamide as the only reaction byproduct of heterocondensation (Fig. 1S†). Templates were removed by calcinations in air at 400 and 500 °C. Heat treatment in the atmosphere of N_2 at 400 and 500 °C was employed as an effective method for carbonization and reduction of Sn species to metallic tin nanoparticles.

IR spectra of dried gels presented in Fig. 1 show vibrational bands corresponding to Si–O–Sn linkages[18,36,37] at 940–956 cm^{-1}, Si–O–Si at 793–799 and 1014–1030 cm^{-1}, and Sn–O–Sn[38] at 667 cm^{-1}. The residual acetoxy groups are represented by asymmetric and symmetric COO stretches at 1564 and 1450 cm^{-1}, respectively. The difference between symmetric and asymmetric carboxylate vibrational bands is 110–120 cm^{-1} and according to Deacon–Phillips rules, this is indicative of their bidentate bridging mode on metal centers.[39] Diethylamido groups display an absorption band at 1370 cm^{-1}. An intense band at 1100 cm^{-1} is attributed to C–O–C vibrations of templates.

TG/DSC analyses of dried products performed under air atmosphere show the highest mass loss between 200 and 400 °C

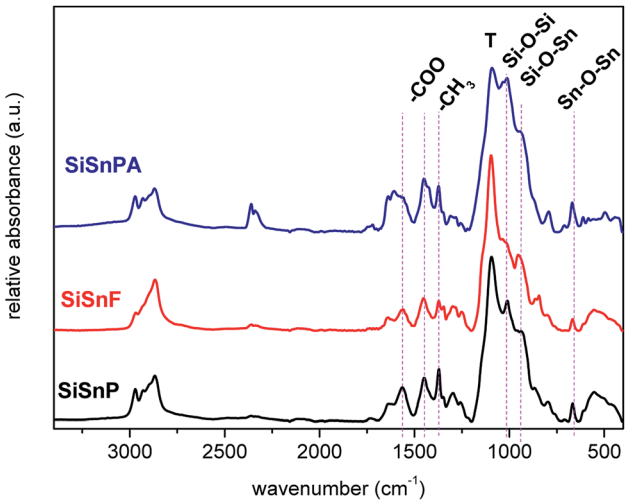

Fig. 1 IR spectra of dried tin silicate xerogels. Vibrational band labeled with T is characteristic for Pluronic templates.

(54–60%). This decrease is caused by oxidation and decomposition of the residual organic groups and templates. An interesting behavior is observed by the DSC method where samples show exothermic peaks between 350 and 400 °C. These effects are attributed to oxidation of copolymer template. Exothermic peak between 400 and 530 °C can be connected with the crystallization of SnO_2 in silicate matrix (Fig. 2 and 2S†). This crystallization effect displayed by the sample SiSnPA (Fig. 3S†) prepared in an autoclave at 110 °C is weaker than in the case of samples SiSnP and SiSnF (Fig. 2S† and 2) synthesized at 80 °C. This may imply better stabilization of Sn in the Sn–O–Si matrix in xerogels prepared by polycondensation at higher temperature. A higher degree of condensation and crosslinking agrees with a lower organic content and thus a higher residual mass left after heating to 1000 °C during the TG/DSC experiments (Table 1). DSC measurements performed in nitrogen atmosphere revealed endothermic peaks between 390 and 410 °C. These effects could correspond to reduction of Sn–O–Si species and subsequent formation of Sn metallic nanoparticles.[40] In the case of SiSnP sample synthesized with P123, the maximum of endothermic peak is located at 399 °C (Fig. 4S†). The DSC curve of SiSnF sample prepared with F127 template shows an exothermic effect followed by an endothermic peak with the maxima at 406 °C (Fig. 2). The SiSnPA DSC curve (Fig. 5S†) of TG/DSC analysis performed under N_2 illustrates weak exothermic and endothermic effects.

Table 1 NHSG reaction parameters and results of TG/DSC experiments

Sample	n_{Si} [mmol]	n_{Sn} [mmol]	Template	$n_{template}$ [mmol]	Residual mass[a] [%] TG air	TG N_2	DC [%]
SiSnP	3.054	3.180	P123	0.181	30.60	30.79	69
SiSnF	2.986	3.018	F127	0.152	21.51	22.93	59
SiSnPA[b]	1.53	1.12	P123	0.067	38.29	38.55	—

[a] After heating to 1000 °C. [b] Reaction in an autoclave.

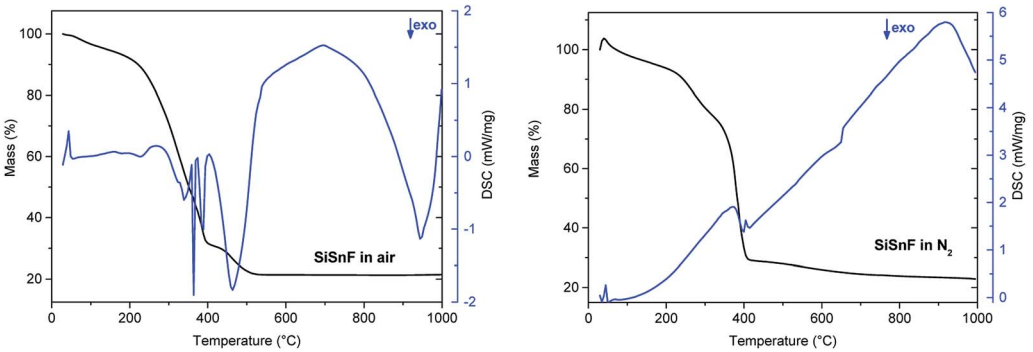

Fig. 2 TG/DSC curves of SiSnF xerogel. Analyses performed in air (left); analyses performed under N_2 (left).

The presence of SnO_2 and metallic Sn particles mentioned above was established by the powder XRD diffraction analysis. The tin silicate xerogels calcined in air at 400 and 500 °C display diffractions of tetragonal cassiterite SnO_2 (PDF 41-1445) (Fig. 3 and 6S†). Considering the width of SnO_2 diffraction lines, the size of crystallites is very small and remains almost constant on heating up to 1200 °C (Fig. 7S, Table 1S†). The Rietveld refinement of the high temperature powder XRD patterns shows an average size of crystallites from 7 to 12 nm (Fig. 7S and 8S†). The size of about 7 nm is retained to 950 °C. A significant increase of the SnO_2 nanoparticle size is observed between 1000 and 1200 °C when the size is increased from 8 to 12 nm (Fig. 7S†). In the case of the autoclave-synthesized sample, SiSnPA-500, SnO_2 nanoparticles with the size of 5.9 nm were observed (Fig. 9S and 10S†). After calcination at 1200 °C the SnO_2 nanocrystal size increased to 8.3 nm (Fig. 11S†). From this behavior we can conclude that the SnO_2 nanocrystals are stabilized to high temperatures as they are enclosed in the pores of silicate matrix and their growth is largely prevented. The powder XRD patterns of the samples heated in N_2 at 500 °C show diffractions assigned to metallic Sn (PDF 04-0673), SnO_2 (PDF 41-1445), and also SnO (PDF 06-0395). The diffractions of metallic tin prove that partial reduction by carbon takes place during heating under N_2 (Fig. 3 and 6S†). The size of Sn nanoparticles in the nanocomposites SiSnF-500N and SiSnPA-500N computed from Rietveld refinement is about 146 and 107 nm, respectively (Fig. 12S and 13S†). Powder XRD diffractogram of the SiSnF-400N sample (heated in N_2 at 400 °C) (Fig. 14S†) does not display the lines of metallic Sn and only weak diffractions of SnO_2 were observed. This result is in an agreement with the DSC measurement where the endothermic effect of Sn reduction is observed at 406 °C. The SnO_2 phase in samples heated under N_2 can be formed by a phase separation from tin silicate during heat treatment.

The solid state NMR spectroscopy was used to study structural sites of calcined xerogels. The ^{29}Si CPMAS NMR spectrum (Fig. 4) of calcined sample SiSnF-500 displays resonances with chemical shifts of −110, −102, and −92 ppm. These signals can be attributed to silicon environments represented by $Si(OSi)_4$, $Si(OSi)_3(OSn)$, and $Si(OSi)_2(OSn)_2$ species (and possibly also Q_3 and Q_2 sites).[41,42] These resonances represent additional hint pointing to the presence of Si–O–Sn bonds in calcined xerogels.

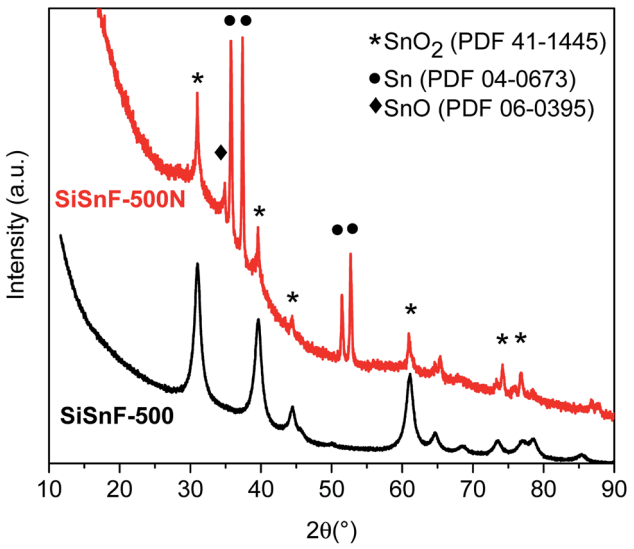

Fig. 3 Powder XRD patterns of calcined xerogels.

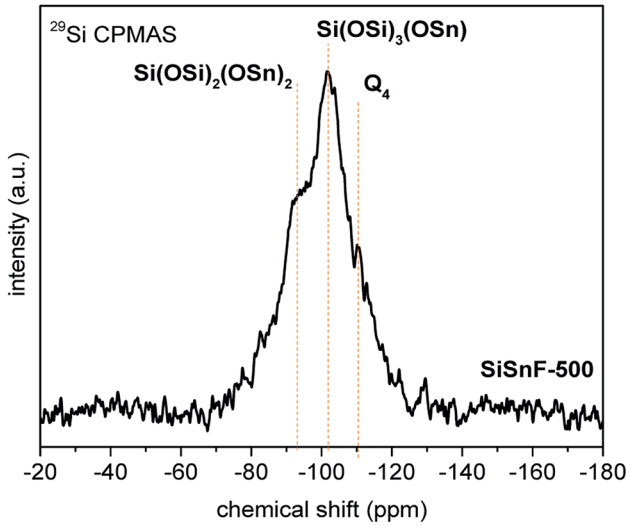

Fig. 4 ^{29}Si CPMAS NMR spectrum of air calcined tin silicate xerogel SiSnF-500.

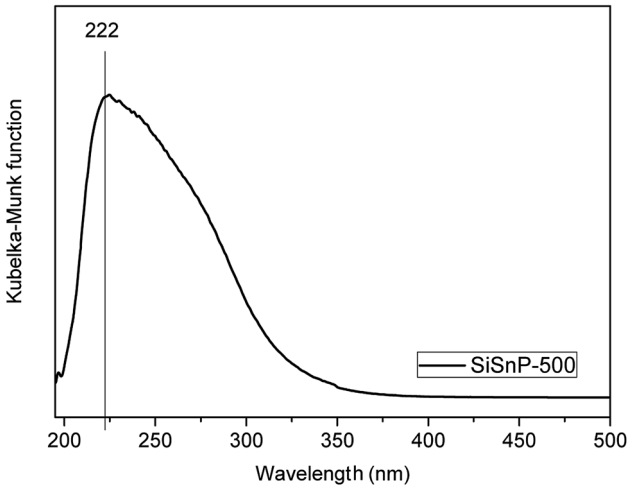

Fig. 5 DRUV-vis spectrum of the sample SiSnP-500.

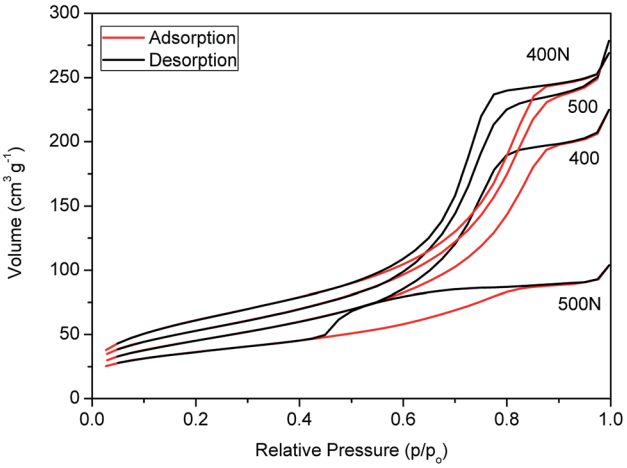

Fig. 6 Adsorption/desorption N_2 isotherms of SiSnF xerogel calcined in air and heated under N_2 at 400 and 500 °C.

The coordination environment of tin centers in the air calcined xerogel SiSnP-500 was examined by DRUV-vis spectroscopy (Fig. 5). Absorption maxima observed at 222 nm are attributed to tetrahedrally coordinated tin atoms.[17,36,37,41] The shoulder at about 266 nm is indicative of hexacoordinated polymeric Sn species. This spectrum indicates that a part of the tin atoms in the calcined xerogels are tetrahedrally coordinated. These species are not separated as SnO_2 after calcination, but form a solid solution of SnO_2 in SiO_2.

Air calcined tin silicate xerogels exhibit surface areas from 164 to 476 $m^2\ g^{-1}$ and total pore volume from 0.28 to 0.58 $cm^3\ g^{-1}$ (Table 2). Adsorption/desorption isotherms belong to type IV with H2 hysteresis at higher p/p_0 pressures, characteristic of mesoporous solids. The average pore diameters reach up to 9.8 nm. The mesopores can be in this case occupied by SnO_2 nanoparticles and this probably accounts for the relatively low pore volumes. On the other hand, their embedding in the pores prevents growth of SnO_2 crystals during heat treatment. The pore diameters are in close agreement with the sizes of SnO_2 nanoparticles computed by Rietveld refinement[33] (Table 1S†). The highest surface area of 476 $m^2\ g^{-1}$ with pore volume of 0.58 $cm^3\ g^{-1}$ and pore diameter of 6.6 nm (Fig. 15S,† Table 2) was reached with the calcined product of the reaction performed in an autoclave (SiSnPA-500). This could be a result of a lower Sn content, more extensive crosslinking due to higher reaction temperature, and resulting higher homogeneity. Moreover, the different polarity of CH_2Cl_2, as compared to toluene, can affect the arrangement of the template in the reaction mixture. After heating under N_2 (500 °C) the sample SiSnPA-500N exhibits specific surface area of 123 $m^2\ g^{-1}$. In this case mesoporosity is retained the average pore diameter is surprisingly higher (9.8 nm) than for the sample calcined in air (SiSnPA-500) (Fig. 16S and 17S†), and also higher than the pore diameters of other N_2 heated samples. This difference could be caused by a lower content of Sn, higher condensation degree and resulting stability of this sample during the heating in N_2, and/or by the formation of a lower amount of SnO_2 as compared to the sample calcined in air. The tin silicate xerogel SiSnF-500N heated under nitrogen at 500 °C exhibits a lower apparent surface area (121 $m^2\ g^{-1}$, 0.14 $cm^3\ g^{-1}$) than the sample calcined in air (Fig. 6). This decrease is caused by reduction of Sn species and separation of Sn nanoparticles. The pore diameter according to QSDFT

Table 2 BET specific surface areas, total pore volumes, and average pore diameters of calcined and N_2 heated xerogels

Sample	Template	SSA (BET) [$m^2\ g^{-1}$]	V_{tot} [$cm^3\ g^{-1}$]	d [nm]
SiSnP-400	P123	189	0.35	9.7
SiSnP-500	P123	167	0.28	9.1
SiSnP-500N	P123	58	0.06	3.8
SiSnF-400	F127	164	0.32	9.8
SiSnF-500	F127	191	0.39	9.8
SiSnF-400N	F127	223	0.39	5.8
SiSnF-500N	F127	129	0.14	3.4
SiSnPA-500	P123	476	0.58	6.6
SiSnPA-500N	P123	123	0.40	9.8

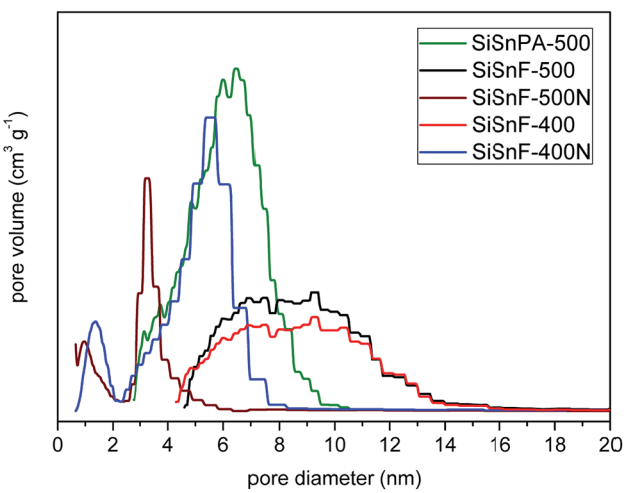

Fig. 7 Pore diameter histograms of SiSnPA and SiSnF xerogels calcined in air (NLDFT) and heated under N_2 (QSDFT).

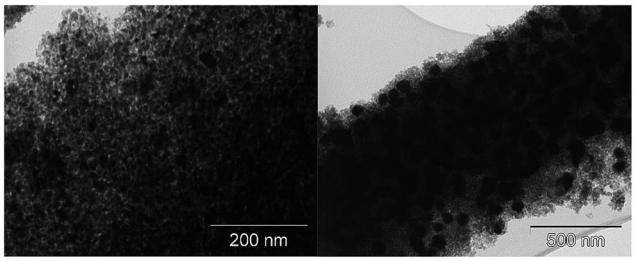

Fig. 8 TEM images of SiSnP sample calcined in air (left) and heated under N_2 (right).

is 3.4 nm and it shows that mesoporous character is retained (Fig. 7). In this case, the hysteresis type is H4 which is characteristic for slit-shaped pores and/or plate-like particles.[43] The same xerogel SiSnF heated in N_2 atmosphere at 400 °C reached a surface area of 223 m^2 g^{-1} (Fig. 6, Table 2). At 400 °C, the xerogel framework does not collapse and Sn species are not reduced to metallic tin nanoparticles. This observation is in a good agreement with the powder XRD pattern where diffractions of metallic tin is not observed at this temperature and the DSC endothermic peak for the metallic Sn formation appears above 406 °C (Fig. 2).

TEM images illustrate the morphology and structure of air calcined and N_2 heated xerogels (at 500 °C). Air calcined xerogels display SnO_2 nanoparticles embedded in silica (Fig. 8 left, Fig. 18S†). Composites formed during heating in N_2 display relatively uniform Sn metallic particles in silica/carbon matrix (Fig. 8 right). The size of these particles is approximately 70–150 nm.

The presence of Lewis and Brønsted acid sites on the surface of air-calcined xerogel (SiSnP-500) was examined by pyridine adsorption followed by IR spectroscopy. Vibrational bands in the IR spectra (Fig. 19S†) were assigned to Lewis (1454 cm^{-1}), Lewis + Brønsted (1489 cm^{-1}) and Brønsted (1540 cm^{-1}) acidic sites.[44] These data indicate that calcined tin-silicate materials possess mixed Lewis and Brønsted surface acidity.

Catalytic studies

The catalytic performance of air-calcined tin silicate xerogels was evaluated in a model reaction of aminolysis of styrene oxide with aniline.[32] For the catalytic tests, 25 mg of a dried (vacuum, 115 °C, 1 h) calcined xerogel was used. Reaction mixtures were analyzed by ^{1}H NMR spectroscopy during the tests. The ^{1}H NMR spectra of the reaction mixture (in C_6D_6) display resonances attributed to two products: 2-phenyl-2-(phenylamino)ethanol (**I**) and 1-phenyl-2-(phenylamino)ethanol (**II**) (Fig. 20S and 21S†). These products were also confirmed by the GC-MS technique. Yields of products were measured after 5, 60, and 120 min. The tin silicate catalysts exhibit a good activity (up to 63%) and high selectivity for the product **I** (Table 3). To the best of our knowledge, there are no reports related to SnO_2–SiO_2 aminolysis catalysts for comparison with our results. However, the Sn-beta zeolite was used to catalyze aminolysis.[45] The details and catalytic activities are given in Table 4. These results show that we achieved comparable conversion and higher selectivity. However, Tang *et al.*[45] used much lower tin content in their catalyst and TON number is therefore increased. The second type of testing reaction was Meerwein–Ponndorf–Verley reduction[3] of 4-*tert*-butylcyclohexanone in isopropanol (Fig. 22S†). The resulting products were analyzed by the GC-MS technique.

Table 3 Aminolysis of styrene oxide. Conversions and selectivities

Sample	Sn [wt%] (ICP)	n_{Sn} in cat [mmol]	SSA (BET) [m^2 g^{-1}]	d [nm]	t [min]	Conversion [%]	Selectivity [%]		TOF[a] [mmol $mmol^{-1}$ h^{-1}]
							I	**II**	
SiSnP-500	52.4	0.11	167	9.1	5	20	97	3	109
					60	50	96	4	23
					120	63	95	5	14
SiSnF-400	43.2	0.09	164	9.8	60	34	95	5	19
SiSnF-500	43.2	0.09	191	9.8	60	30	96	4	17

[a] Apparent turnover frequency TOF [mmol $mmol^{-1}$ h^{-1}].

Table 4 Aminolysis of styrene oxide with aniline Sn-beta zeolite catalysts[a,45]

Catalyst	n_{Si}/n_M	Conversion [%]	Selectivity [%]		TON[b] [$mmol_{Epo}$ $mmol_M^{-1}$]
			I	**II**	
Sn-beta[45]	97.0	25.4	91.0	9.0	305.0
Meso-Sn-beta[45]	96.8	41.0	91.1	8.9	476.0

[a] Reaction conditions: 5 mmol epoxide, 5 mmol amine, 25 mg catalyst, temperature = 35 °C, reaction time = 0.5 h. [b] Calculated as the number of moles of styrene oxide converted per mole of the metal center.

In this case we observed 1-isopropoxy-4-*tert*-butylcyclohexane[46] (yield 7%) instead of the 4-*tert*-butylcyclohexanol as the expected product (Fig. 23S†). This could be caused by the presence of Brønsted active sites on the catalyst.

Conclusions

In this work we presented a novel non-hydrolytic templated acetamide elimination as an efficient one-pot sol–gel method for the preparation of tin silicate xerogels with a high content of tin (up to 52.4 wt%). The polycondensation reaction provides homogeneous transparent stiff gels containing Si–O–Sn linkages and releases *N*,*N*-diethylacetamide as the condensation byproduct. Addition of Pluronics P123 and F127 as templates and gelation agents to the reaction mixture was crucial for achieving mesoporous character of xerogels and for preventing pore collapse upon calcination. We also demonstrated the use of autoclave in these reactions and this modification brings the advantage of lower organic residual content and provides higher condensation degree. By varying the heat treatment conditions, the synthesized gels were processed to two types of materials. On one hand, calcination in air atmosphere leads to mesoporous SnO_2–SiO_2 xerogels with surface areas up to 476 m^2 g^{-1} and containing stabilized SnO_2 nanoparticles with the size of ~6 nm. Their diameter remains constant even up to 950 °C and only increases to ~12 nm at 1200 °C. Air calcined xerogels were tested as catalysts for aminolysis of styrene oxide and featured 63% conversion after 2 h. Catalysis of MPV reduction of 4-*tert*-butylcyclohexanone resulted in the 1-isopropoxy-4-*tert*-butylcyclohexane (7%) as a catalytic product instead of expected alcohol.

On the other hand, heating in N_2 atmosphere resulted in the Sn–silica–carbon nanocomposites. These materials display mesoporous character with a small amount of micropores. The size of Sn particles is in the range of 70–150 nm. Potential application of these nanocomposites could be found in electrode materials.[47]

From these data we can conclude that non-hydrolytic templated acetamide elimination can be used as an effective one pot synthetic method for the preparation of SnO_2–SiO_2 and Sn–silica–carbon nanocomposites.

Acknowledgements

This research has been financially supported by the Ministry of Education, Youth and Sports of the Czech Republic under the project CEITEC 2020 (LQ1601). Authors thank L. Simonikova for ICP-OES analyses, L. Krauskova for DRUV-vis spectroscopy, Professor Z. Travnicek (UPOL) for CHN analysis, and Johan G. Alauzun for helpfull discussion and assistance.

References

1 X. Wang, H. Xu, X. Fu, P. Liu, F. Lefebvre and J.-M. Basset, *J. Mol. Catal. A: Chem.*, 2005, **238**, 185–191.
2 A. Corma, M. A. T. Navarro and M. Renz, *J. Catal.*, 2003, **219**, 242–246.
3 A. Corma, M. E. Domine and S. Valencia, *J. Catal.*, 2003, **215**, 294–304.
4 H. J. Cho, P. Dornath and W. Fan, *ACS Catal.*, 2014, **4**, 2029–2037.
5 W. R. Gunther, Y. Wang, Y. Ji, V. K. Michaelis, S. T. Hunt, R. G. Griffin and Y. Román-Leshkov, *Nat. Commun.*, 2012, **3**, 1109.
6 S. Samanta, N. K. Mal, A. Manna and A. Bhaumik, *Appl. Catal., A*, 2004, **273**, 157–161.
7 E. Taarning, S. Saravanamurugan, M. Spangsberg Holm, J. Xiong, R. M. West and C. H. Christensen, *ChemSusChem*, 2009, **2**, 625–627.
8 J. Yang, K. Hidajat and S. Kawi, *J. Mater. Chem.*, 2009, **19**, 292–298.
9 N. R. Srinivasan and R. Bandyopadhyaya, *Microporous Mesoporous Mater.*, 2012, **149**, 166–171.
10 N. R. Srinivasan, P. Majumdar, N. K. R. Eswar and R. Bandyopadhyaya, *Appl. Catal., A*, 2015, **498**, 107–116.
11 K. Bachari and O. Cherifi, *Appl. Catal., A*, 2007, **319**, 259–266.
12 K. R. Reddy, M. Suresh, M. L. Kantam, S. K. Bhargava and P. Srinivasu, *Ind. Eng. Chem. Res.*, 2014, **53**, 18630–18636.
13 Y.-C. Chen, J.-M. Chen, Y.-H. Huang, Y.-R. Lee and H. C. Shih, *Surf. Coat. Technol.*, 2007, **202**, 1313–1318.
14 C.-M. Yang, P.-H. Liu, Y.-F. Ho, C.-Y. Chiu and K.-J. Chao, *Chem. Mater.*, 2003, **15**, 275–280.
15 N. K. Mal, A. Bhaumik, R. Kumar and A. V. Ramaswamy, *Catal. Lett.*, 1995, **33**, 387–394.
16 B. Tang, W. Dai, G. Wu, N. Guan, L. Li and M. Hunger, *ACS Catal.*, 2014, **4**, 2801–2810.
17 S. Endud and K.-L. Wong, *Microporous Mesoporous Mater.*, 2007, **101**, 256–263.
18 R. Rajalakshmi, V. V. Srinivasan, M. P. Pachamuthu and R. Maheswari, *Mater. Chem. Phys.*, 2015, **154**, 164–169.
19 D. P. Debecker, V. Hulea and P. H. Mutin, *Appl. Catal., A*, 2013, **451**, 192–206.
20 D. P. Debecker and P. H. Mutin, *Chem. Soc. Rev.*, 2012, **41**, 3624–3650.
21 A. Vioux, *Chem. Mater.*, 1997, **9**, 2292–2299.
22 P. H. Mutin and A. Vioux, *Chem. Mater.*, 2009, **21**, 582–596.
23 P. Kirszensztejn, A. Kawałko, A. Tolińska and R. Przekop, *J. Porous Mater.*, 2010, **18**, 241–249.
24 C. Leonhardt, S. Brumm, A. Seifert, G. Cox, A. Lange, T. Rüffer, D. Schaarschmidt, H. Lang, N. Jöhrmann, M. Hietschold, F. Simon and M. Mehring, *ChemPlusChem*, 2013, **78**, 1400–1412.
25 A. Aboulaich, B. Boury and P. H. Mutin, *Eur. J. Inorg. Chem.*, 2011, **2011**, 3644–3649.
26 A. Styskalik, D. Skoda, J. Pinkas and S. Mathur, *J. Sol-Gel Sci. Technol.*, 2012, **63**, 463–472.
27 D. Skoda, A. Styskalik, Z. Moravec, P. Bezdicka, C. Barnes and J. Pinkas, *J. Sol-Gel Sci. Technol.*, 2015, **74**, 810–822.
28 D. Skoda, A. Styskalik, Z. Moravec, P. Bezdicka and J. Pinkas, *J. Mater. Sci.*, 2015, **50**, 3371–3382.
29 D. Skoda, A. Styskalik, Z. Moravec, P. Bezdicka, M. Babiak, M. Klementova, C. E. Barnes and J. Pinkas, *RSC Adv.*, 2016, **6**, 24273–24284.

30 J. H. Balthis, E. G. Rochow and D. G. White, in *Inorganic Syntheses*, John Wiley & Sons, Inc., 2007, pp. 45–47.
31 Z. Zhao, Y. Liu, H. Wu, X. Li, M. He and P. Wu, *Microporous Mesoporous Mater.*, 2009, **123**, 324–330.
32 R. Kore, R. Srivastava and B. Satpati, *ACS Catal.*, 2013, **3**, 2891–2904.
33 H. Rietveld, *J. Appl. Crystallogr.*, 1969, **2**, 65–71.
34 J. Rouquerol, F. Rouquerol, P. Llewellyn, G. Maurin and K. S. W. Sing, *Adsorption by Powders and Porous Solids: Principles, Methodology and Applications*, Elsevier Science, 2013.
35 S. Lowell, J. Shields, M. Thomas and M. Thommes, in *Characterization of Porous Solids and Powders: Surface Area, Pore Size and Density*, Springer, Netherlands, 2004, vol. 16, ch. 5, pp. 58–81.
36 K. Chaudhari, T. K. Das, P. R. Rajmohanan, K. Lazar, S. Sivasanker and A. J. Chandwadkar, *J. Catal.*, 1999, **183**, 281–291.
37 M. P. Pachamuthu, K. Shanthi, R. Luque and A. Ramanathan, *Green Chem.*, 2013, **15**, 2158–2166.
38 A.-M. Ungureanu, O. Oprea, B. Vasile, C. Andronescu, G. Voicu and I. Jitaru, *Cent. Eur. J. Chem.*, 2014, **12**, 909–917.
39 G. Deacon and R. Phillips, *Coord. Chem. Rev.*, 1980, **33**, 227–250.
40 C. Leonhardt, S. Brumm, A. Seifert, A. Lange, S. Csihony and M. Mehring, *ChemPlusChem*, 2014, **79**, 1440–1447.
41 M. Sasidharan, Y. Kiyozumi, N. K. Mal, M. Paul, P. R. Rajamohanan and A. Bhaumik, *Microporous Mesoporous Mater.*, 2009, **126**, 234–244.
42 P. Shah, A. V. Ramaswamy, K. Lazar and V. Ramaswamy, *Microporous Mesoporous Mater.*, 2007, **100**, 210–226.
43 G. Leofanti, M. Padovan, G. Tozzola and B. Venturelli, *Catal. Today*, 1998, **41**, 207–219.
44 K. Raveendranath Reddy, D. Venkanna, M. Lakshmi Kantam, S. K. Bhargava and P. Srinivasu, *Ind. Eng. Chem. Res.*, 2015, **54**, 7005–7013.
45 B. Tang, W. Dai, X. Sun, G. Wu, N. Guan, M. Hunger and L. Li, *Green Chem.*, 2015, **17**, 1744–1755.
46 M. J. Verhoef, E. J. Creyghton and J. A. Peters, *Chem. Commun.*, 1997, 1989.
47 J. Hwang, S. H. Woo, J. Shim, C. Jo, K. T. Lee and J. Lee, *ACS Nano*, 2013, **7**, 1036–1044.